Telecommunications and Radio Engineering, 79(1):1-16 (2020)

APPLIED RADIO PHYSICS

TROPOSPHERIC SCINTILLATION EFFECTS ON SATELLITE LINKS FROM X-BAND TO Q-BAND OVER NIGERIAN CLIMATIC ZONES USING KARASAWA AND ITU-R MODELS

O.F. Dairo,* A.A. Willoughby, S.O. Adesanya, & L.B. Kolawole

Redeemer's University, P.M.B. 230, Ede, Osun State 232102, Nigeria

*Address all correspondence to: O.F. Dairo, E-mail: dairof@run.edu.ng

The tropospheric scintillation of satellite communication signals has continued to draw the attention of radio engineers. The effect and prevalent paucity of Earth-space tropospheric scintillation data in Africa are remarkable. The parameters of NigComSat-1R and Eutelsat-36B satellites were used for this modeling from X- to Q-band during the West African monsoon (WAM). The low error rates of Karasawa and ITU-R models reported for the tropical climates made them appropriate for this study. In situ data from the Tropospheric Data Acquisition Network stations spanning three climatic regions in Nigeria, namely Tropical Monsoon, Geo. 6.5º N, 3.5º E; Tropical Savanna, Geo. 8.99º N, 7.38º E; and the Sahel, Geo. 9.35º N, 12.5º E. The scintillation variability is lowest in the tropical monsoon climate and highest in the Sahel climate using both models. However, the ITU-R model recorded higher scintillation fade depths (SFDs) of 37.19 dB, 2.91 dB, and 2.52 dB, for low elevation, NigComSat-1R and Eutelsat-36B satellites respectively, over the tropical monsoon climatic zone, than Karasawa model, which recorded SFDs of 34.07 dB, 1.31 dB, and 1.09 dB for the respective satellites. The observed scintillation intensity increased with increasing carrier frequency, low elevation angle and small receiving antenna. High variability of the scintillation intensity characterizes the onset of WAM and post-monsoon months.

KEY WORDS: *tropospheric scintillation, fade depth, satellite communication, scintillation intensity, microwave, tropical climate, radio refractivity*

1. INTRODUCTION

The prevalence of Earth-space communication over other means of radio propagation has increased the horizon of its services beyond fixed satellite services (FSS) and intercontinental radiocommunication services. The other services include

environmental monitoring, astronomy, remote sensing, augmented reality and a host of others. Consequently, many military applications depend on satellite communication for real-time information exchange. However, the availability and reliability of satellite communication networks have challenged its use in the surge of evolving and emerging applications [1-5].

The introduction of Earth-space links in the lower region of the microwave band was well received and barely experienced inconsiderable radio propagation impairment at frequencies less than 10 GHz [6]. On the other hand, the accompanying overriding financial implication of the antennas due to the large aperture of about (~30 m) and wind loading short-lived the excitement. Soon the C-band slot of the geostationary earth orbit (GEO) became congested laden with interference. The overcrowding led to the exploration of the mid microwave frequencies from K (12 GHz) to Q (50 GHz) bands [1,7,8]. The higher frequency bands paved the way for new applications and broader market segments of the digital economy, namely smart grid, transport system logistics and e-health. Associated with higher frequency bands virtues of larger bandwidth, smaller antenna size and higher throughput is the liability of atmospheric impairments. Aside from the attenuation of satellite communication signals due to the absorption lines of atmospheric gases, scintillation is an impairment that increases remarkably with increasing frequency. This impairment, observed as the fluctuation of the received signal intensity about its threshold, is known as scintillation enhancement or fades [9-14].

Scintillation is the rapid fluctuations of the amplitude, angle of arrival, phase, and polarization of the received signal as a result of the irregularities in space and time of the constitutive parameters of the transmission medium. The troposphere, consisting of the highly convective atmospheric boundary layer (ABL), is a lossy medium for radio waves propagation. Hence, tropospheric scintillation is due to the marked fluctuations of the refractive index within the ABL [8]. This variability is a result of a high humidity lapse rate and temperature inversion layers. The spatial-temporal variability, which depends on the local climate, is both seasonal and diurnal with evidence of latitudinal variation. The observed chaotic mixing of air parcels in the equatorial region [15-18] and its stochastically varying climatic evolutions in space and time [19,20] during the West African Monsoon (WAM) regime, starting from the pre-monsoon to the post-monsoon [21-23], have continued to beam the searchlight on scintillation in the region [7,8]. The prevalence of high solar insolation and the monsoon circulation in the equatorial latitudes have characterized its climate as hot, humid and highly convective [24]. WAM drives the forced convection observed with turbulence and thunderstorms over the West African coast. Hence the deep convection is a result of the interplay of these processes in equatorial tropics.

A large chunk of the observations and efforts to study scintillation have been in the temperate region: USA [11,25-28], Canada [29,30], Norway [31], UK [32,33], and Europe [34-36]. The deficit of direct-to-home optical fiber infrastructure within Nigeria has made many to rely on satellite point-to-point and point-to-multipoint services for banking, automated teller machine, upstream oil and gas exploration, direct-to-home broadcasting, among others. The erratic nature of these satellite

services has left in its wake, sometimes, long queues in the banking hall and dismayed football fans due to degradation of the received satellite signal [12], to mention a few.

Models predicting scintillation intensity as a function of the variance of signal log-amplitude have been reported to be more accurate for the tropical climate [37-40]. Hence Karasawa and ITU-R models, from which other models have been formulated and modified for certain climates, were chosen [41]. Also, low-elevation satellites, at an angle of $\theta = 5°$ covering the tropics, were considered. As a result, this study used meteorological data to consider the seasonal patterns of frequency, elevation angle and latitudinal variation of scintillation effects on two prominent satellites over the equatorial climatic zone. The two satellites are the Nigerian communication satellite-1 replacement - NigComSat-1R and Eutelsat 36B - used by digital satellite television (DSTV), a major commercial satellite broadcasting company in Africa.

2. METHODOLOGY

Space and time variability of scintillation intensity over Nigeria was modeled using meteorological parameters. The data input were obtained in situ from the three major climate zones using the Tropospheric Data Acquisition Network (TRODAN) stations in Lagos, Abuja and Yola (Table 1). TRODAN, formerly known as the Nigerian Environmental Climatic Observing Program (NECOP), is being executed by the National Space Research and Development Agency (NASRDA) in collaboration with the Centre for Climatic Research, Delaware, United States, Nigerian Meteorological Agency (NiMET) and Nigerian Universities. The project commenced in 2007 with capacity training at Centre for Climatic Research (CCR), Delaware, United States, where an engineer was trained on the implementation of a mandate to replicate the CCR kind of system in Nigeria.

TABLE 1: Location, climate and satellite elevation

Station	Geo. Coordinate	Climate	NigComSat-1R	EutelSat 36B
Lagos	6.5°N, 3.5°E	Monsoon	44.2°E	51.4°E
Abuja	8.99°N, 7.38°E	Tropical savanna	48.1°E	55.1°E
Yola	9.35°N, 12.5°E	Sahel	53.5°E	60.5°E

The three stations are in the tropical monsoon, tropical savanna and Sahel climates. These climatic zones, with the Atlantic boundary in the south and the Sahelian boundary in the north, are typical of the latitudinal variation across Nigeria. The derivative of the meteorological parameters is used to characterize compute scintillation intensity of X- to Q-band (10 GHz–50 GHz) [1,42]: the standard deviation, σ, of the log-amplitude; the variance, σ^2; the amplitude deviation y in dB; and the predicted variance, σ_p^2 [43-47] for NigComSat-1R and Eutelsat 36B (Table 2).

TABLE 2: Satellite Data

Satellite	NigComSat-1R	EutelSat 36B
Application	Communication	Communication
Equipment	4 C-, 14 ku-, 8 ka-, 2 L-bands	70 ku-bands
Orbit	GEO	GEO
Location	42.5°E	35.9°E
Operator	NASRDA	Eutelsat

3. SCINTILLATION MODELS

Tropospheric scintillation models derive their indicators from the statistics of the relevant meteorological parameter. These estimates are the cumulative distribution function (CDF), the probability density function (PDF) and the variance of the log-amplitude fluctuation [9]. The key component of scintillation models is the assumption that the log-amplitude fluctuation follows a Gaussian probability distribution function for the short-term [43]. Hence the models are classified as either predicting the variance or lognormal distribution of scintillation. For the long-term, the International Telecommunication Union - Radiocommunication (ITU-R) model is widely used because of the global inputs in its development and the Karasawa model for being the foremost [40,41,47-51]. These models use the wet term of the surface radio refractivity, N_{wet} [48,52], as an input parameter, to estimate the standard deviation of satellite signal fluctuation contributed by scintillation. High error rates characterize other tropospheric scintillations models when considered for the tropics. In particular, they were originally developed for the temperate climates and as such unreliable for tropical climates [40,41,53]. Most of these models were chiefly fine-tuned for European climates with very low N_{wet} .

3.1 Karasawa Model

The averaged monthly standard deviation of the signal level, $m = \langle \sigma_X \rangle$ is estimated using [8,47,54]

$$m = \sigma_{X,ref} \cdot \eta_f \cdot \eta_\theta \cdot \eta_{D_e} \ (\mathrm{dB}), \tag{1}$$

where the radio refractivity dependent term of the standard deviation of the reference signal amplitude, $\sigma_{X,ref}$ in (1) is scaled by 0.0228 and expressed as [8,41,49]

$$\sigma_{X,ref} = 0.15 + 5.2 \times 10^{-3} N_{wet} \ (\mathrm{dB}), \tag{2}$$

the frequency-dependent term, η_f, n_f

$$\eta_f = \left(\frac{f}{11.5}\right)^{0.45} \tag{3}$$

the elevation angle-dependent term, η_θ,

$$\eta_\theta = \left(\sin 6.5^o / \sin\theta\right)^{1.3}. \qquad \text{for } \theta \geq 5^o, \tag{4a}$$

$$\eta_\theta = \left(2\sin 6.5^o \Big/ \left[\sqrt{\sin^2\theta + \frac{2h}{R_e}} + \sin\theta\right]\right)^{1.3}, \qquad \text{for } \theta < 5^o, \tag{4b}$$

where the effective Earth's radius, R_e = 8500 km at sea level and the turbulence height, h = 2 km the antenna aperture size term, η_{Da}, is the antenna averaging function and expressed as [55]

$$\eta_{Da} = \sqrt{\frac{GD_{eff}}{G(7.6)}}, \tag{5}$$

where

$$G\left(D_{eff}\right) = 1.0 - 0.7\left(\frac{D_{eff}}{\sqrt{\lambda L}}\right) \qquad \text{for } 0 \leq \frac{D_{eff}}{\sqrt{\lambda L}} \leq 1.0, \tag{6a}$$

$$G\left(D_{eff}\right) = 0.5 - 0.2\left(\frac{D_{eff}}{\sqrt{\lambda L}}\right) \qquad \text{for } 1.0 < \frac{D_{eff}}{\sqrt{\lambda L}} \leq 2.0, \tag{6b}$$

$$G\left(D_{eff}\right) = 0.1 \qquad \text{for } 2.0 < \frac{D_{eff}}{\sqrt{\lambda L}} \tag{6c}$$

$$\lambda = c / f \ \ (\text{m})$$

$$D_{eff} = \sqrt{\eta D} \ \ (\text{m})$$

$$L = 2h \Big/ \left(\sqrt{\sin^2\theta + 2h / R_e} + \sin\theta\right)(\text{m}), \tag{7}$$

where c is the speed of light in free space (m/s), f is the frequency (GHz), λ is the wavelength (m), θ is the free-space elevation angle (degrees), D is the antenna diameter (m), D_{eff} is the effective antenna diameter (m),L is the effective path length, which is the turbulent layer distance from the receiver (m).

The monthly cumulative distribution of amplitude variation y is expressed in the terms of the predicted monthly standard deviation. The expression is deduced from the integral of the short-term distribution function of the standard deviations with the conditional distribution function of the short-term signal level y given standard deviation, where both are respectively distributed Gamma and Gaussian [14,54]. In other words, the short-term PDF of the log-amplitude is normally distributed. The predicted amplitude deviation exceeded, given a time $p\%$, for signal fade $As(p)$ (exceeded for the time $p\%$) is derived from (8)

$$y = As(p) = a(p) \cdot m \ \ (\mathrm{dB}). \tag{8}$$

For scintillation enhancement exceeded for the time $p\%$ is predicted as

$$Es(p) = e(p) \cdot m. \tag{9}$$

The time percentage factor enhancement for $0.01\% \le p \le 50.0\%$ is expressed as

$$e(p) = -0.0597(\log_{10} p)^2 - 1.258\log_{10} p + 2.672. \tag{10}$$

The fade for $0.01\% \le p \le 50.0\%$ is expressed as

$$a(p) = -0.061(\log_{10} p)^3 - 0.072(\log_{10} p)^2 1.71\log_{10} p + 3.0. \tag{11}$$

3.2 ITU-R Model

The model [51], which is analogous to the Karasawa model, yields the predicted standard deviation of the signal for the applicable period and propagation path as (12)

$$\sigma = \sigma_{ref} f^{7/12} \frac{g(x)}{(\sin\theta)^{1.2}}, \tag{12}$$

where the standard deviation of the reference signal amplitude, σ_{ref}, is expressed as (13)

$$\sigma_{ref} = 3.6\times10^{-3} + N_{wet}\times10^{-4} \ (\mathrm{dB}). \qquad (\mathrm{dB}). \tag{13}$$

The antenna averaging factor, $g(x)$, is given by (14)

$$g(x) = \sqrt{3.86(x^2+1)^{11/12} \cdot \sin\left[\frac{11}{6}\tan^{-1}\frac{1}{x}\right] - 7.08x^{5/6}}, \tag{14}$$

$$x = 1.22 D_{eff}^2 \left(\frac{f}{L} \right), \tag{15}$$

where θ = free-space elevation angle, for $\theta \geq 5^o$.

Equation (14) is only valid for $x \prec 7.0$, otherwise, the predicted scintillation fade depth for any time percentage is zero.

The fade depth, $A(p)$, surpassed for the time percentage ($p\%$) is expressed as (16)

$$A(p) = a(p) \cdot \sigma \ (\text{dB}), \tag{16}$$

where the time percentage fade factor, $a(p)$, in the range of $0.01\% \prec p \leq 50\%$ is given by (11).

4. RESULTS AND ANALYSIS

The climatology of the scintillation intensity of earth-space signals in the troposphere over Nigeria is observed to be seasonally, elevation and frequency-dependent. Similarly, the seasonal variability is also climatic and latitudinally dependent. The variance distribution showed a marked increasing trend of scintillation intensity from the Sahel climate in the high latitudes to the monsoon climate in the low latitudes. Hence, it is a reflection of the inward flow of the monsoon from the Atlantic cold tongue in the south and migrating through the tropical savanna in the middle-belt to the prevalent Sahel climatic condition in the north.

4.1 Variability in the Tropical Monsoon

The tropical monsoon showed quasi-sinusoidal distributions of scintillation fade depth (SFD) as a function of the standard deviation of signal fluctuation. Figures 1–3 showed that both models coincide with the time-dependence of tropospheric scintillation. March showed seasonal peaks of scintillation fade for all frequencies and August the dips. These maxima correspond to insolation maximum occurring during the spring equinox over the monsoon climate [24]. Consequently, the increased solar activity corresponds to increased chaoticity in the troposphere, which is characteristic of the onset of the harmattan-rainy transition phase (HRTP) [15-17,52,56]. Also, Figs. 1–3 showed the frequency dependence of scintillation fade along its trajectories. The effect of the equatorial monsoonal climate on the gradient of intensity variability for both ITU-R and Karasawa models is 9%. For low-elevation satellites $\left(\theta \leq 5^o\right)$ the intensity of tropospheric scintillation ranged from 22.85 dB to 34.07 dB for the Karasawa model and 13.58 dB to 37.41 dB for the ITU-R model. On the other hand, the scintillation intensity is considerably lower for an antenna aimed at the two commercial satellites

over the African continent, namely NigComSat-1R and Eutelsat 36B. For antenna aimed at Eutelsat 36B, scintillation intensity varied from a minimum of 0.75 dB to a maximum of 1.09 dB for ITU-R and from 0.96 dB to 2.52 dB for Karasawa. The variability ranged from 1.10 dB to 2.91 dB for ITU-R and from 0.90 dB to 1.31 dB Karasawa for antenna aimed at NigComSat-1R.

4.2 Variability in the Tropical Savanna

A quasi-cyclic distribution was observed in the trend of scintillation intensity over the tropical savanna. According to Figs. 4–6, the degree of convergence of the distribution is higher in the Karasawa model than that of the ITUR model during the harmattan rainy transition phase (HRTP), where the scintillation fade depth converged for both models. The HRTP ushered in a significant phase change, which coincides with the increased solar activity due to the interplay between the retreat of the harmattan wind known as tropical continental air mass (cT) and the onset of the pre-monsoonal rainy wind known as tropical maritime air mass (mT) [52]. The scintillation variability is highest during HRTP, March to April, leading to increased chaoticity [15–17,56], as a result of the northward swing of the Intertropical Convergence Zone (ITCZ) over Nigeria at this period. The swing trails the northward migration of the sun, which is driving the low-pressure regime. The pre-monsoonal scintillation intensity in April is sustained over the tropical savanna by the arrival and retreat of the tropical monsoon up to October. The minima are observed in January and March whiles the maxima in August and September. The maxima of scintillation intensity indicate the onset of the southward migration of the sun. Hence the autumn equinox, which is responsible for the second wave of high insolation over the equator [24,57]. Approximately 50% coefficient of variation is observed for both models.

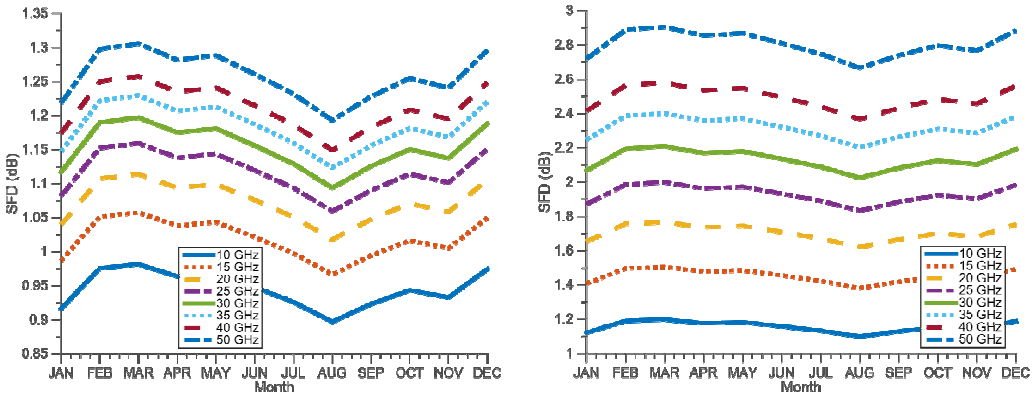

a) b)

FIG. 1: SFD of NigComSat-1R signal over Lagos (Geo. 6.5°N, 3.5°E) at an elevation angle, $\theta = 44.2°$, for (a) Karasawa and (b) ITU-R models

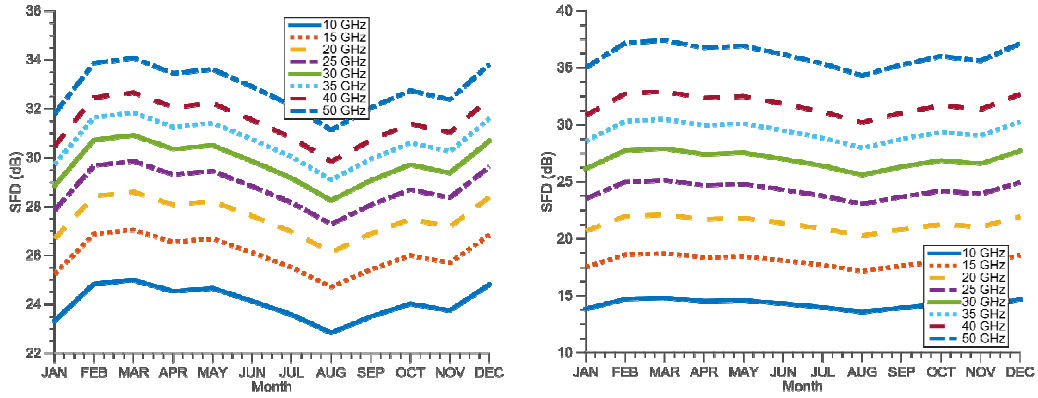

a) b)

FIG. 2: SFD of low-elevation satellite signal over Lagos (Geo. 6.5°N, 3.5°E) at an elevation angle, θ= 5°, for (a) Karasawa and (b) ITU-R models

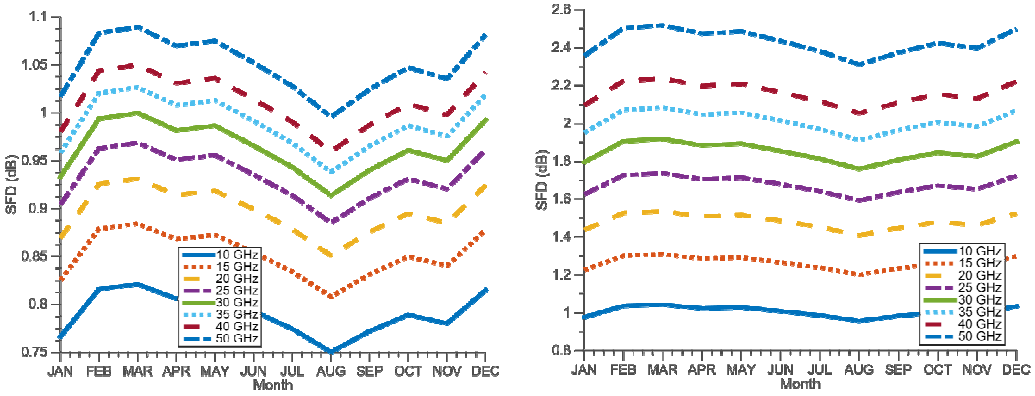

a) b)

FIG. 3: SFD of Eutelsat signal over Lagos (Geo. 6.5°N, 3.5°E) at an elevation angle, $\theta = 51.4^{o}$, for (a) Karasawa and (b) ITU-R models

At an elevation of 5°, the depth of fade intensity varies from 9.14 dB to 34.65 dB for both models. The low elevation fade depths are comparable to rain attenuation [9,58,59]. On the other hand, at an elevation of 48.1°, for antenna aimed at NigComSat-1R, the fade depth ranges between 0.53 dB and 2.48 dB for models. Correspondingly, for antenna aimed at Eutelsat 36B, the fade depth varies from 0.46 dB to 2.19 dB for both models.

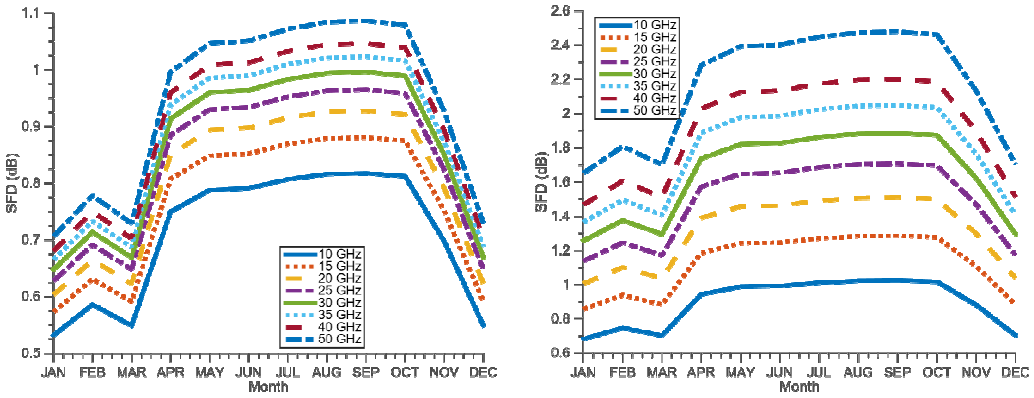

a) b)

FIG. 4: SFD of NigComSat-1R signal over Abuja (Geo. 8.99°N, 7.38°E) at an elevation angle, $\theta = 48.1°$, for (a) Karasawa and (b) ITU-R models

4.3 Variability in the Sahel

Figures 7–9 showed the distributions of the variability of scintillation fade intensity in the Sahelian climate over Nigeria, for both ITU-R and Karasawa models. The trend of the standard deviation of link variability is typical of the boundaries of the Sahel in the south. The scintillation intensity minima were observed in March during the HRTP, while the maxima in August before the rainy-harmattan transition phase (RHTP).

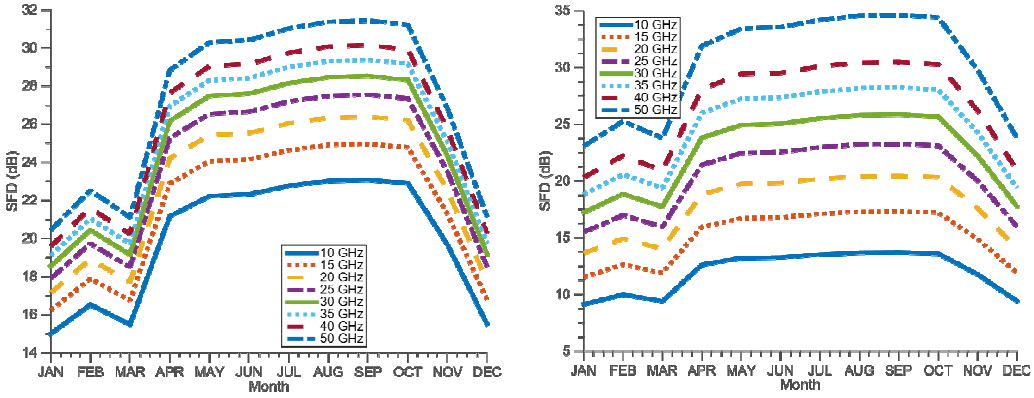

a) b)

FIG. 5: SFD of low-elevation satellite signal over Abuja (Geo. 8.99°N, 7.38°E) at an elevation angle, $\theta = 5°$, for (a) Karasawa and (b) ITU-R models

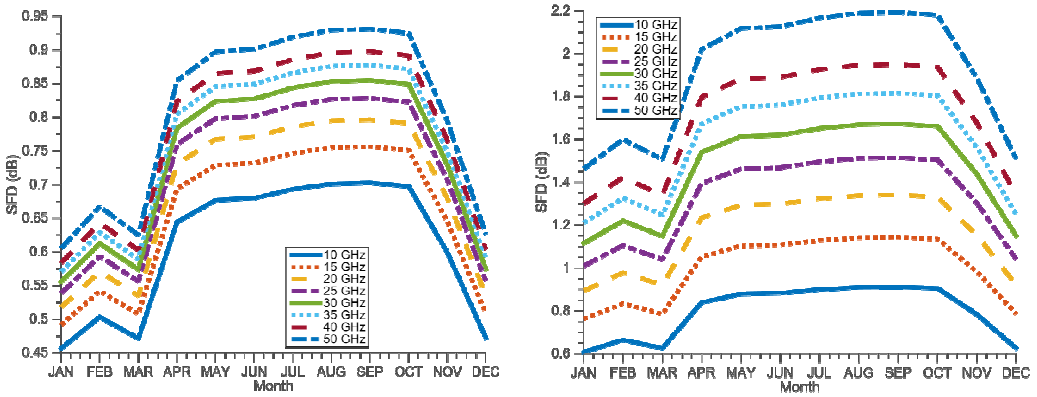

FIG. 6: SFD of Eutelsat signal over Abuja (Geo. 8.99°N, 7.38°E) at an elevation angle, $\theta = 55.1°$, for (a) Karasawa and (b) ITU-R models

The minima (dip) prevailed throughout the harmattan period, from November to March. Both the minima in March and the maxima occurred during the period of increased insolation over the Sahel. The onset of the pre-monsoon mT between March and April is characterized by a positive gradient of fade depth variability, leading to increased chaoticity [15-17,56]. The maxima correspond to the rainy period in the Sahel, from June to September. The June solstice ushers in the Sahel rainy season, which consequently leads to the autumn equinox characterized by increased solar activities during the southern migration of the sun over the equatorial latitudes [24]. The gradient of variability is between ~158% and ~180% for ITU-R and Karasawa models, respectively.

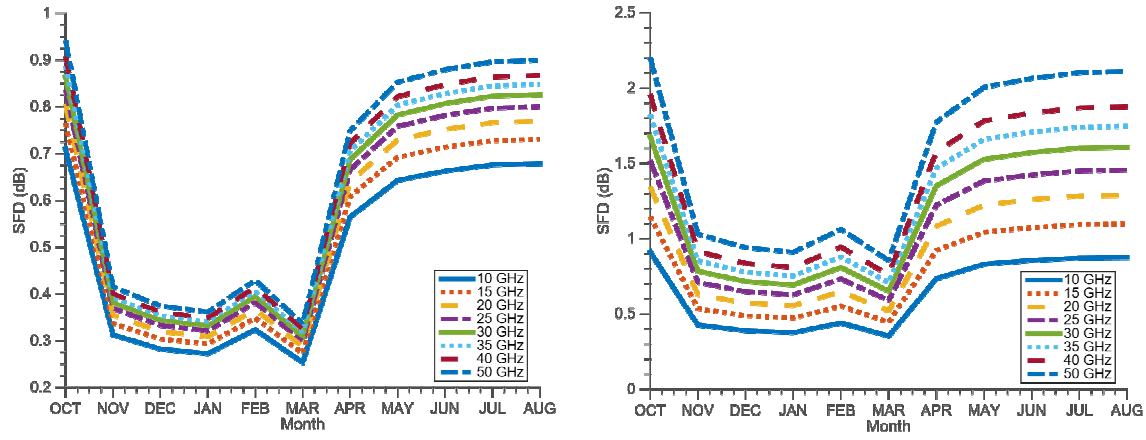

FIG. 7: SFD of NigComSat-1R signal over Yola (Geo. 9.35°N, 12.5°E) at an elevation angle, $\theta = 53.5°$, for (a) Karasawa and (b) ITU-R models

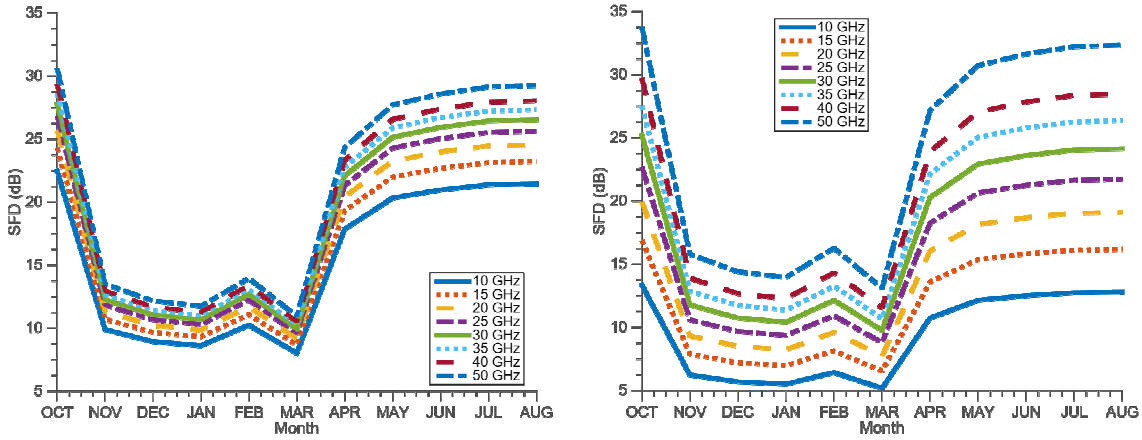

a) b)

FIG. 8: SFD of low-elevation satellite signal over Yola (Geo. 9.35°N, 12.5°E) at an elevation angle, θ= 5°, for (a) Karasawa and (b) ITU-R models

At an elevation of θ ≤ 5°, the intensity of fade depth varies between 5.19 dB and 33.77 dB for both models. However, for an antenna looking at NigComSat-1R, the range of the SFD is between 0.25 dB and 2.20 dB for both ITU-R and Karasawa models. Likewise, the SFD fluctuates between 0.22 dB and 1.98 dB for both models, for an antenna aimed at Eutelsat 36B.

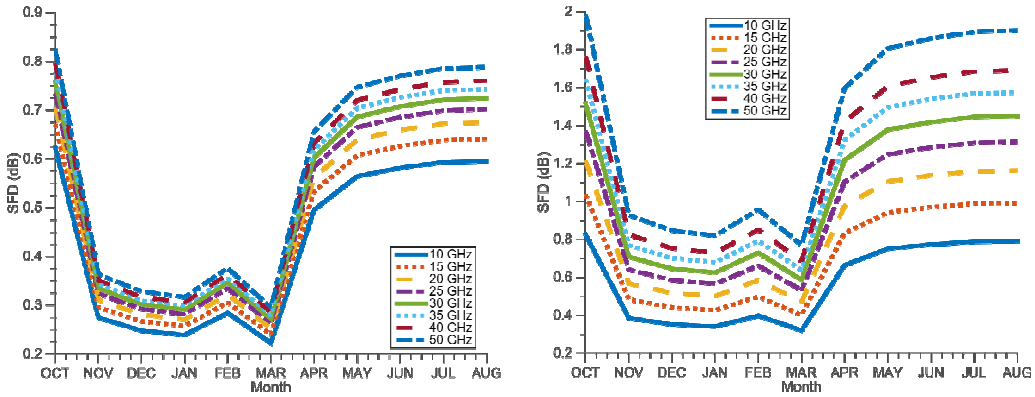

a) b)

FIG. 9: SFD of Eutelsat-DSTV signal over Yola (Geo. 9.35°N, 12.5°E) at an elevation angle, θ = 60.5°, for (a) Karasawa and (b) ITU-R models

5. CONCLUSION

The variability of the predicted tropospheric SFD, derived from the monthly variance of the signal log-amplitude, is both space- and time-dependent. Hence, the latitudinal variations and the prevailing tropical climatic conditions characterize the SFD distributions. In particular, the low latitudes showed the strongest intensity of SFD, while the high latitudes showed the weakest intensity. Similarly, for antennas aimed at NigComSat-1R and Eutelsat 36B, the ITU-R model predicted higher SFD compared to the Karasawa model. On the other hand, low-elevation satellites recorded a trend reversal, where the long-term SFD predicted by the ITU-R model were considerably lower than those predicted by the Karasawa model up to 35 GHz at 99.99% availability required service level agreements (SLAs) for communication backbones. Also, from 40 GHz to 50 GHz, the ITU-R model reported higher values than that of Karasawa. In general, both models predicted higher values of SFD intensities at low elevation, which are comparable to the attenuation impairment induced by rain. The monsoon climate predicted the highest SFD intensities of 2.52 dB, 2.91 dB and 37.19 dB at elevation angles of 51.4°, 44.2° and 5° for antenna aimed at Eutelsat, NigComSat-1R and low-elevation satellites, respectively, using the ITU-R model. Correspondingly, 1.09 dB, 1.31 dB and 34.07 dB were obtained using the Karasawa model. Also, increasing elevation angles were observed for both Eutelsat and NigComSat-1R latitudinally, from the tropical monsoon to the tropical Sahel.

The results show that the SFD increases with the increasing carrier frequency, decreasing the elevation angle and decreasing the size of the receiving antenna. High variability of the SFD characterizes the onset of WAM and post-monsoon months (PMM). The variability converges during the transition phases, HRTP and RHTP. The frequency-dependent dispersion is lower during the harmattan period than the period from the onset of WAM to the peak of WAM.

Generally, the ITU-R model predicted higher effects of tropospheric scintillation on satellite signals than the Karasawa model, with the lowest dispersion in the lower bands. Hence, the sensitivity of the ITU-R model to frequency is higher than that of the Karasawa model. However, the Karasawa model recorded the highest variability of SFD. Moreover, the variability is highest in the Sahel climate compared with the tropical savanna and monsoon climates.

High solar activity in the tropics is responsible for the low-pressure regimes in the African equatorial region, which in turn drives the turbulence observed over the region. Therefore, ground stations of tropospheric scintillation are necessary for radio engineers to map the climatology of SFD effects over the African equatorial region for optimization of the existing models. Results such as these may significantly improve future ITU-R recommendations, which will, in turn, lead to improved Earth-space links performance in the tropics.

ACKNOWLEDGMENTS

The authors would like to thank the National Space Research and Development Agency (NASRDA) and the Centre for Basic Space Science (CBSS), Nsukka, Nigeria

for the data, support and approval to access the Tropospheric Data Acquisition Network (TRODAN).

REFERENCES

1. Mrak, S., Hrovat, A., Vidmar, M., and Vilhar, A., (2018) A discrete-components millimeter-wave satellite beacon receiver for q-band propagation experiment, *International Journal of Satellite Communications and Networking*, **36**(4), pp. 372-382. doi:10.1002/sat.1240.
2. Ajiboye, A., Abdulrahman, A., Falade, A., Ajiboye, A. et al., (2017) Effects of ionospheric scintillation on communication systems: Gps and satellite, *Telecommunications and Radio Engineering*, **76**(20), pp. 1849-1859. doi:10.1615/TelecomRadEng.v76.i20.50.
3. Dairo, O.F. and Kolawole, L.B., (2017) Statistical Analysis of Tropospheric Scintillation of Satellite Communication Signals using Karasawa and ITU-R Models, *IEEE 3rd International Conference on Proceedings- Electro-Technology for National Development NIGERCON*, (ISSN 2377-2697), pp. 347-352. doi:https://doi.org/10.1109/NIGERCON.2017.8281906.
4. Maral, G. and Bousquet, M., (2010) *Satellite Communications Systems: Systems, Techniques and Technology*, John Wiley and Sons Ltd, Hoboken, United States.
5. Pratt, T., Bostian, C., and Allnutt, J., (2003) *Satellite Communications*, John Wiley and Sons, Inc., New York.
6. Stutlman, W.L. and Chakraborty, D., (1992) The Olympus and ACTS propagation measurement campaigns in the U.S., *14th International Communication Satellite Systems Conference and Exhibit held at*, Washington DC, pp. 1435-1439.
7. Allnut, J.E. and Rogers, D.V., (1989) Low-fade-margin systems: propagation considerations and implementation approaches, *6th International Conference on Antennas and Propagation (ICAP' 89),* pp. 6-9.
8. Ippolito, L.J., (2008) *Satellite Communications Systems Engineering: Atmospheric Effects, Satellite Link Design, and System Performance*, John Wiley & Sons, Sussex, U.K.
9. Luini, L., Riva, C., Emiliani, L., and Nessel, J., (2019) Modeling the Impact of Rain and Clouds on Earth-Space Site Diversity Systems, *IEEE Transactions on Antennas and Propagation*, **67**(1), pp. 475-483. doi:10.1109/TAP.2018. 2876712.
10. Cox, D.C., Arnold, H.W., and Hoffman, H.H., (1981) Observation of Cloud-Produced Amplitude Scintillation on 19- and 28-GHz Earth-Space paths, *Radio Science*, **17**(5), pp. 885-907.
11. Hinder, R.A., (1970) Observations of atmospheric turbulence with a radio telescope, *Nature*, **225**, pp. 614-617.
12. Karasawa, Y. and Matsudo, T., (1991) Characteristics of fading on low-elevation angle earth-space paths with concurrent rain attenuation and scintillation, *IEEE Trans. Ant. Prop*., **39**, pp. 657-661.
13. Otung, I.E. and Savvaris, A., (2006) Estimating tropospheric scintillation intensity on earth-space propagation paths, *Elec. Let*., **42**(7), pp. 381-382.
14. Otung, I.E. and Evans, B.G., (1995) Short Term Distribution of Amplitude Scintillation on a Satellite Link, *Electronics Letters*, **31**(16), pp. 1328-1329.
15. Ojo, J., Adelakun, A., and Edward, O., (2019) Comparative study on radio refractivity gradient in the troposphere using chaotic quantifiers, *Heliyon*, **5**(8), p. e02083. doi:https://doi.org/10.1016/j.heliyon.2019.e02083.
16. Adeniji, A.E., Olusola, O.I., and Njah, A.N., (2018) Comparative study of chaotic features in hourly wind speed using recurrence quantification analysis, *AIP Advances*, **8**(2), pp. 025102. doi:10.1063/1.4998674.
17. Ogunsua, B., Ojo, J., and Adediji, A., (2018) Atmospheric chaoticity and complexity from radio refractivity derived from Akure station, *Advances in Space Research*, **62**(7), pp. 1690-1701. doi:https://doi.org/10.1016/j.asr2018.06.035.
18. Strohbehn, J.W., (1968) Line-of-sight wave propagation through the turbulent atmosphere, *Proc. of the IEEE*, **56**(8), pp. 1301-1318.

19. Fang, D.J., (1980) 4/6 GHz ionospheric scintillation measurements, *AGARD Conf. Proc. 284 Propagation Effects in Space/Earth Paths 33*, pp. 1-12.
20. Haddon, J. and Vilar, E., (1986) Scattering induced microwave scintillations from clear-air and rain on earth-space paths and the influence of antenna aperture, *IEEE Trans. AP*, **34**, pp. 646-651.
21. Vellinga, M., Arribas, A., and Graham, R., (2010) Seasonal forecasts for regional onset of the West African Monsoon, *Clim. Dyn.*, **40**, pp. 3047-3070. URL https://doi.org/10.1007/s00382-012-1520-z.
22. Brandt, P., Caniaux, G., Bourles, B., Lazar, A. et al., (2011) Equatorial upper-ocean dynamics and their interaction with the West African monsoon, *Atmos. Sci. Lett*., **12**, pp. 24-30.
23. Coetlogon, G.D., Janicot, S., and Lazar, A., (2010) Intraseasonal variability of the ocean - atmosphere coupling in the Gulf of Guinea during boreal spring and summer, *Q. J. R. Meteorol. Soc*., **136**, pp. 426-441. URL https://doi.org/10.1002/qj.554.
24. Akala, A.O., Amaeshi, L.L.N., Somoye, E.O., Idolor, R.O. et al., (2015) Climatology of gps amplitude scintillations over equatorial Africa during the minimum and ascending phases of solar cycle 24, *Astrophysics and Space Science*, **357**(1), pp. 1-17. doi:10.1007/s10509-015-2292-9.
25. Webber, R.V. and McCormick, K.S., (1980) Low elevation angle measurements of the ATS-6 beacons at 4 and 30 GHz, *Ann. Telecomm*., **35**, pp. 1n-7n.
26. Vogel, W.J., Straiton, A.W., and Fannin, B.M., (1977) Ats-6 ascending: near horizon measurements over water at 30 GHz, *Radio Science*, **12**, pp. 757-765.
27. Stutlman, W.L., Bostian, C.W., Manus, E.A., Marshall, R.E., and Wiley, P.H., (1975) ATS-6 satellite 20 GHz propagation measurements at low elevation angles, *Electronics Letters*, **11**, pp. 635-636.
28. McCormick, K.S. and Maynard, L.A., (1971) Low angle tropospheric fading in relation to satellite communications and broadcasting, *Int. Conf. on Comm. ICC-7I-CIC*, **12**, pp. 12.18-12.23.
29. Lam, W.I., (1988) Low angle signal fading at 38 GHz in the high Arctic, *IEEE Trans. AP*, **35**, pp. 1495-1499.
30. Strickland, J.I., Olsen, R.I., and Westiuk, H.L., (1977) Measurement of low angle fading in the Canadian Arctic, *Ann. Telecomm*., **32**, pp. 530-535.
31. Osen, O., (1980) Propagation effects in high latitudes, *Proc. International Symposium on Symphonie*, pp. 415-423.
32. Otung, I.E., Mahmoud, M.S., and Norbury, J.R., (1995) Radiowave amplitude scintillation intensity: Olympus satellite measurements and empirical model, *Electronics Letters*, **31**(21), pp. 1873-1875.
33. Otung, I.E., Mahmoud, M.S., and Norbury, J.R., (1995) Differential amplitude scintillation in a Ka-band satellite link, *International Conference on Antennas & Propagation (ICAP 95),* Eindhoven, Netherlands, **407**(2), pp. 85-88.
34. Haidara, F.M., Bostian, C.W., and Pratt, T., (1994) Measurements of tropospheric scintillations on a 14-degree path at 12, 20, and 30 GHz, *AIAA-94*, pp. 921-931.
35. Vanhoenacker, D. and Poirares Baptista, J.P.V., (1994) Atmospheric scintillation, in: *OPEX Reference Book on Attenuation Measurement and Prediction*, ESA WPP-083, pp. 51-64.
36. Ortgies, G., (1993) Frequency dependence of slant-path amplitude scintillations, *Elec. Let*., **29**(25), pp. 2219-2220.
37. Akinwumi, S., Omotosho, T., Usikalu, M., Adagunodo, T. et al., (2018) Analysis and comparison of tropospheric scintillation prediction models at covenant university, *IOP Conference Series: Earth and Environmental Science*, **173**(1). doi:10.1088/1755-1315/173/1/012015.
38. Madhuri, A., Immadi, G., and Narayana, M., (2018) Estimation of cumulative distribution of scintillation effect on Ku band frequencies for one of the tropical regions using various models, *Journal of Engineering Science and Technology Review*, **11**(1), pp. 151-155.
39. Rabiul Hossain, M., Uddin, N., Zafar Md Imran, A., Jashim Uddin, M., and Gafur, A., (2018) Comparative analysis on tropospheric scintillation prediction models for Bangladeshi climate, *Int. Conference on Innovations in Science, Engineering and Technology, ICISET*, pp. 412-417.
40. Mandeep, J. and Zali, R., (2011) Analysis and comparison model for measuring tropospheric scintillation intensity for Ku-band frequency in Malaysia*, Earth Sciences Research Journal*, **15,** pp. 13-17.
41. Chen, C.Y. and Singh, M.J., (2014) Comparison of tropospheric scintillation prediction models of the Indonesian climate, *Earth, Planets and Space*, **66**(1), p. 64. doi:10.1186/1880-5981-66-64.

42. Vanhoenacker-Janvier, D., Quibus, L., Rytir, M., and Tjelta, T., (2017) Measurement and modeling of tropospheric scintillation in Ka/Q band, *11th European Conference on Antennas and Propagation, EUCAP*, pp. 1486-1490. doi:10.23919/EuCAP.2017.7928514.
43. Gimonet, M.E., Van De Kamp, M.M.J.L., Marzano, F.S., Riva, C., and Salonen, E.T., (2002) Cost Action 255: Radiowave Propagation Modelling for SatCom Services at Ku-Band and Above Final Report, *European Space Agency*, *Ch. Scintillation/Dynamics of the signal*, pp. 1-11.
44. Van De Kamp, M.M.J.L., Tervonen, J.K., Salonen, E.T., and Poirares Baptista, J.P.V., (1999) Improved models for long-term prediction of tropospheric scintillation on slant paths, *IEEE Trans. Ant. Prop*., **47**(2), pp. 249-260.
45. Tervonen, J.K., Van De Kamp, M.M.J.L., and Salonen, E.T., (1998) Prediction Model for the Diurnal Behavior of the Tropospheric Scintillation Variance, *IEEE Transactions on Antennas and Propagation*, **46**(9), pp. 1372-1378.
46. Peetters, G., Marzano, F.S., d'Auria, G., Riva, C., and Van Hoenacker-Janvier, D., (1997) Evaluation of Statistical Models for Clear-Air Scintillation Prediction Using Olympus Satellite Measurements, *International Journal of Satellite Communications*, **15**, pp. 73-88.
47. Karasawa, Y., Yasukawa, K., and Yamada, M., (1988) Tropospheric scintillation in the 14/11-GHz bands on Earth-space paths with low elevation angles, *IEEE Trans. Ant. Prop*., **36**(4), pp. 563-569.
48. ITU-R P.453-13, The radio refractive index: Its formula and refractivity data, Tech. rep., ITU, Geneva, Switzerland (2017).
49. Harris, R.A., (2002) *Cost Action 255: Radiowave Propagation Modelling for SatCom Services at Ku-Band and Above Final Report*, COST 255 Final Report, SP-1252 ISBN 92-9092-608-2., European Space Agency, Brussels.
50. Marzano, F.S. and d'Auria, G., (1998) Model-based prediction of amplitude scintillation variance due to clear-air tropospheric turbulence on Earth-satellite microwave links, *IEEE Trans. Ant. Prop*., **46**(10), pp. 1506-1518.
51. ITU-R P.618-12, Propagation data and prediction methods required for the design of Earth-space telecommunication systems, Tech. rep., ITU, Geneva, Switzerland (2015).
52. Dairo, O.F. and Kolawole, L.B., (2018) Radio refractivity gradients in the lowest 100 m of the atmosphere over Lagos, Nigeria in the rainy-harmattan transition phase, *Journal of Atmospheric and Solar-Terrestrial Physics*, **167,** pp. 169-176. doi:https://doi.org/10.1016/j.jastp.2017.12.001.
53. Ojo, J.S., Rabiu, B., Radicella, S.M., and Obiyemi, O.O., (2018) Experimental analysis and comparison of tropospheric scintillation prediction models using eutelsat-36b satellite in a tropical Nigeria, *International Journal of Basic and Applied Sciences*, **7**(1), pp. 8-14.
54. Karasawa, Y., Yamada, M., and Allnut, J.E., (1988) A new prediction method for tropospheric scintillation on Earth-space paths, *IEEE Trans. Ant. Prop*., **36**(11), pp. 1608-1614.
55. Crane, R.K. and Blood, D.W., (1979) *Handbook for the Estimation of Microwave Propagation Effects*, Technical Report No°1 Doc. 7376- TR1, NASA Contract NAS5-25341, NASA GSFC Greenbelt, MA, USA (June 1979).
56. Adelakun, A., Ojo, J., and Edward, O., (2019) Quantitative analyses of complexity and nonlinear trend of radio refractivity gradient in the troposphere, *Advances in Space Research.* doi:https://doi.org/10.1016/j.asr.2019.09.055.
57. Omotosho, T.V., Akinwumi, S.A., Usikalu, M.R., Ometan, O.O., and Adewusi, M.O., (2016) Tropospheric scintillation and its impact on earth-space satellite communication in Nigeria, *IEEE Radio and Antenna Days of the Indian Ocean (RADIO)*, pp. 1-2. doi:10.1109/RADIO.2016.7772041.
58. Abdulrahman, Y., Rahman, T.A., Islam, R.M., Olufeagba, B.J., and Chebil, J., (2015) Comparison of measured rain attenuation in the 10.982-GHz band with predictions and sensitivity analysis, *International Journal of Satellite Communications and Networking*, **33**(3), pp. 185-195, sAT-13-0013.R1. doi:10.1002/sat.1082.
59. Shrestha, S. and Choi, D.-Y., (2017) Rain attenuation statistics over millimeter-wave bands in South Korea, *Journal of Atmospheric and Solar-Terrestrial Physics*, **152**(Supplement C), pp. 1-10. doi:https://doi.org/10.1016/ j.jastp.2016.11.004.